Therapeutics, Targets, and Chemical Biology

Cancer Research

Efficient Tumor Targeting with High-Affinity Designed Ankyrin Repeat Proteins: Effects of Affinity and Molecular Size

Christian Zahnd[1,2], Martin Kawe[1,2], Michael T. Stumpp[1,2], Christine de Pasquale[3], Rastislav Tamaskovic[1], Gabriela Nagy-Davidescu[1], Birgit Dreier[1], Roger Schibli[3], H. Kaspar Binz[1,2], Robert Waibel[3], and Andreas Plückthun[1]

Abstract

Slow-clearing, tumor-targeting proteins such as monoclonal antibodies typically exhibit high tumor accumulation but low tissue contrast, whereas intermediate-sized proteins such as scFvs show faster clearance but only moderate tumor accumulation. For both, tumor targeting does not seem to improve further above an optimal affinity. We show here that with very small high-affinity proteins such as designed ankyrin repeat proteins (DARPins), these limits can be overcome. We have systematically investigated the influence of molecular mass and affinity on tumor accumulation with DARPins with specificity for HER2 in SK-OV-3.ip nude mouse xenografts. DARPins with a mass of 14.5 kDa and affinities between 270 nmol/L and 90 pmol/L showed a strong correlation of tumor accumulation with affinity to HER2, with the highest affinity DARPin reaching 8% ID/g after 24 hours and 6.5% ID/g after 48 hours (tumor-to-blood ratio >60). Tumor autoradiographs showed good penetration throughout the tumor mass. Genetic fusion of two DARPins (30 kDa) resulted in significantly lower tumor accumulation, similar to values observed for scFvs, whereas valency had no influence on accumulation. PEGylation of the DARPins increased the circulation half-life, leading to higher tumor accumulation (13.4% ID/g after 24 hours) but lower tumor-to-blood ratios. Affinity was less important for tumor uptake of the PEGylated constructs. We conclude that two regimes exist for delivering high levels of drug to a tumor: small proteins with very high affinity, such as unmodified DARPins, and large proteins with extended half-life, such as PEGylated DARPins, in which the importance of affinity is less pronounced. *Cancer Res; 70(4): 1595–605. ©2010 AACR.*

Introduction

Therapeutic antibodies have been used in recent years for the targeting of solid tumors (1–3) to overcome the lack of specificity of classic anticancer drugs. Even though human antibodies are now available through a variety of technologies (4), the clinical efficacy of even some marketed antitumor antibodies is limited (5, 6), suggesting that additional effector mechanisms will be needed (1, 7). This argues for the construction of novel robust targeting molecules which can be engineered for enhanced efficacy, e.g., by facile linkage to additional effector molecules. For any effector function that could exert toxicity on normal cells, high tumor localization of the targeting molecule and sufficiently rapid elimination from healthy tissue is pivotal.

Tumor targeting proteins seem to be caught between two constraints. Slow-clearing, tumor-targeting proteins such as monoclonal antibodies with long half-lives typically exhibit high tumor accumulation but low tissue contrast (8). Intermediate-sized proteins such as scFvs show faster clearance but only moderate tumor accumulation (9, 10). It has been suggested that very high affinities might not be beneficial for increased targeting in either case (11, 12).

We show here that with very small high-affinity proteins such as designed ankyrin repeat proteins (DARPins), these limits can be overcome, and we present a systematic approach that establishes the observed tumor accumulation and targeting contrast as a function of affinity, targeting molecule size, and pharmacokinetics.

HER2-overexpressing breast tumors are well studied and thus represent a suitable reference point for evaluating alternative binding molecules in tumor localization studies. The overexpression of HER2 is correlated with an aggressive tumor phenotype (13) and it occurs in a broad range of human cancers, notably breast and ovarian cancers (14, 15). HER2 is a 185 kDa transmembrane glycoprotein receptor tyrosine kinase of the family of human epidermal growth factor receptors (HER; refs. 16, 17). It plays a key role in HER ligand–dependent tumor growth and could form different

Authors' Affiliations: [1]Universität Zürich, Biochemisches Institut, Winterthurerstrasse, Zürich, Switzerland; [2]Molecular Partners AG, Schlieren, Switzerland; and [3]Center of Radiopharmaceutical Sciences, Paul Scherrer Institut, Villigen PSI, Switzerland

Note: Supplementary data for this article are available at Cancer Research Online (http://cancerres.aacrjournals.org/).

C. Zahnd, M. Kawe, and M.T. Stumpp contributed equally to this work.

Corresponding Author: Andreas Plückthun, Biochemisches Institut, Winterthurerstrasse 190, 8057 Zürich, Switzerland. Phone: 41-44-635-5570; Fax: 41-44-635-5712; E-mail: plueckthun@bioc.uzh.ch.

doi: 10.1158/0008-5472.CAN-09-2724

types of heterodimers with other family members, notably HER3 (16, 18).

Recently, we have developed combinatorial libraries of a new class of small proteins, termed "designed ankyrin repeat proteins" (19, 20) that can act as an alternative to antibodies, as they are particularly robust to engineering. They are based on a very different structure (Supplementary Fig. S1) and are built from consecutive 33-amino acid repeats, each forming a β-turn followed by two antiparallel α-helices. In each repeat, seven residues were randomized, and these internal repeats are flanked by constant capping repeats, to give one contiguous polypeptide chain with a randomized binding surface. The proteins contain no cysteine, can be expressed in soluble form in the cytoplasm of *Escherichia coli* at very high levels, and are very stable and resistant to aggregation (ref. 21 and references therein). By attaching a polyethylene glycol (PEG) molecule (22), the hydrodynamic radius of DARPins can be optionally increased dramatically, thus altering the pharmacokinetic profile of the DARPin to a longer half-life. DARPins can also easily be engineered in the form of homodimers and heterodimers, trimers, or even higher multimers (Supplementary Fig. S1), as well as in the form of other fusion proteins, all in soluble form and with the same high yield from *E. coli*.[4]

High-affinity binders against a wide variety of targets and in particular HER2-specific DARPins have previously been selected from our DARPin libraries both by ribosome and phage display (23–25). From this latter work, we have isolated point mutants of a specific anti-HER2 DARPin (molecular weight, 14.5 kDa) showing affinities between 90 pmol/L and 270 nmol/L. Here, we use these DARPins in tumor-targeting experiments, showing that unmodified high-affinity DARPins, having a very fast clearance, reach high values of tumor accumulation for an extended time with high tumor-to-blood ratios, paralleled by high tumor-to-tissue ratios (except in the liver and kidney, which are involved in excretion). Tumor accumulation correlates with the affinity of these DARPins, without reaching a plateau. With PEG-ylation of the DARPins, even higher tumor accumulation could be achieved, but the slower clearance reduces the tumor-to-blood ratio, and the importance of affinity is significantly less pronounced.

We discuss these results in view of previous studies with antibody fragments of different formats, and also compare them with DARPin constructs engineered to a similar size as scFv fragments.

Materials and Methods

Protein expression and purification. All details are described in the Supplementary Methods and Figs. S2 to S4. Briefly, all DARPin constructs were expressed in *E. coli* XL1-Blue and purified essentially as previously described (24). For PEGylation of the DARPins, a cysteine was introduced at the penultimate position and the protein was allowed to react with maleimide-PEG of 20, 40, or 60 kDa. The scFv fragment 4D5 was expressed and purified in *E. coli* SB536 as previously described (26). HER2 (first 631 amino acids of the mature protein) was kindly provided by Dr. Tim Adams and coworkers (CSIRO, Melbourne, Australia).

His-tag–specific ^{99m}Tc-labeling of the DARPins. The radioactive labeling of the DARPins with $^{99m}Tc(CO)_3$ at the His-tag was performed essentially as previously described (ref. 27; Supplementary Methods).

Tumor cell lines. For all biodistribution studies, the human ovarian carcinoma cell line SK-OV-3.ip was used (kindly provided by Ellen Vitetta, University of Texas, Dallas, TX). For some cell binding experiments and control biodistribution studies, SK-OV-3 (HTB-77; European Collection of Animal Cell Cultures, Salisbury, United Kingdom) and BT474-cells (HTB-20) were also used where indicated.

Affinity-determination of DARPins on human BT474 tumor cells. DARPin-superfolder-GFP fusions were constructed and binding to cells was measured by fluorescence-activated cell sorting by following the on-rate and the off-rate and calculating K_D as their ratio (Supplementary Figs. S5-S6). To minimize internalization, cells were preincubated with 0.2% NaN_3 for 30 min at 37°C. To minimize rebinding during the dissociation phase, a large excess (50 nmol/L) of unlabeled DARPin G3 was added as competitor.

Biodistribution studies of DARPins. Female CD1-FOXn1/nu mice (Charles River), 6 to 8 wk old, were engrafted with human SK-OV-3.ip tumor cells subcutaneously injected at the lateral flanks (10^6 cells, mixed with BD Matrigel Matrix HC; BD Biosciences). The studies were started 2 to 3 wk after tumor inoculation, when the tumors had reached a size of 50 to 300 mg. Each mouse received a single dose of 8 to 10 μg of $^{99m}Tc(CO)_3$-labeled DARPin variant (37 MBq/mouse) intravenously, administered in 100 μL. Mice ($n = 3$ per time point and construct) were sacrificed after 1, 4, 24, 48, and 72 h after injection, organs were removed and the accumulated radioactivity was measured in a gamma-scintillation counter (Supplementary Methods).

Tumor autoradiography. Twenty-four hours after 10 μg (37 MBq) of the $^{99m}Tc(CO)_3$-labeled DARPin variant injection, the SK-OV-3.ip tumors (0.5 cm diameter) were cut into three layers (rim, middle section, rim). The slices were put on a Kodak X-Omat Blue film for 4 h and also analyzed with a Packard InstantImager.

Single photon emission computed tomography imaging studies. Single photon emission computed tomography (SPECT) imaging experiments were performed with an X-SPECT system (Gamma Medica, Inc.) with a single head SPECT device and a computed tomography (CT) device, 24 h after injection of the $^{99m}Tc(CO)_3$-labeled DARPin. The DARPin (370–555 MBq/200 μL = 10–15 mCi/200 μL) was administered via a lateral tail vein (further details in the Supplementary Methods).

For high-resolution images, tumors were scanned with a pinhole collimator (tungsten-based collimator, 1 mm diameter). The SPECT field of view was reduced to 30 × 30 mm and the acquisition time was increased to 4 h.

[4] Kawe et al., unpublished experiments.

Results

Constructs and labeling. In this study, we investigated how efficiently DARPins could be enriched at a tumor site, and determined their biodistribution as a function of affinity and hydrodynamic size. We used a previously described DARPin specific for HER2, i.e., H10-2-G3 (24), or G3 in short. It has a molecular weight of 14.5 kDa and consists of an NH_2-terminal capping repeat, two internal repeats carrying the binding residues, and a COOH-terminal capping repeat (Supplementary Fig. S1). Being derived from an affinity maturation experiment, we could construct the presumed progenitor and its evolutionary intermediates. We therefore had at our disposal DARPins binding to the same epitope on HER2, with affinities ranging from 90 pmol/L to 270 nmol/L. They are named by indicating the amino acid(s) exchanged in G3 (ref. 24; Supplementary Fig. S1).

We expressed these DARPins in *E. coli* and purified them as described (19, 20). They were monomeric on gel filtration (Supplementary Fig. S2) and were labeled with $^{99m}Tc(CO)_3$ on the NH_2-terminal His-tag (27).

The proteins were also derivatized with PEG of different sizes (20–60 kDa) at a unique engineered COOH-terminal cysteine (Supplementary Figs. S3-S4). The PEG20-containing proteins eluted at an apparent molecular weight of >300 kDa, consistent with the well-known effect of PEG20 of greatly increasing the hydrodynamic radius (26, 28). PEGylation had previously been shown to have no effect on the off-rate and only a small effect on the on-rate (28). These PEGylated proteins were ^{99m}Tc-labeled in the same way (27).

For a direct comparison to single-chain Fv fragments, we created DARPins with similar molecular weight as scFvs (~25 kDa): the DARPin G3 was linked via a flexible linker to a nonbinding DARPin, E2_5 (20), or alternatively, to another DARPin G3 to create a bivalent DARPin (Supplementary Fig. S1). These constructs, denoted G3-E2_5 and G3-G3, were expressed, purified, and ^{99m}Tc-labeled as described above.

The stability of the DARPins was tested in PBS and serum. Even after 4 weeks at 37°C, no aggregation, degradation or loss of binding was detected (Supplementary Figs. S7-S10).

Affinities on cells. Previously reported affinities had been measured on purified HER2 by surface plasmon resonance (24). Because the epitope recognized by G3 is on domain-4, proximal to the membrane (17), and because the measured affinity of the monovalent trastuzumab scFv or Fab fragment (also binding to domain-4) is significantly different between purified HER2 and whole cells (28–30), we measured the affinity of the DARPins to whole cells (Supplementary Figs. S5-S6).

We used the mean fluorescence intensity of DARPin-GFP fusions measured by fluorescence-activated cell sorting to determine both on- and off-rates on BT474-cells (Supplementary Figs. S5-S6) under conditions in which receptor internalization is minimized, and from this, we calculated the functional affinity. This approach can be used over a wide range of affinities and allows accurate comparisons even though an effect of GFP cannot strictly be excluded.

The values obtained very closely match those determined with the pure HER2 by surface plasmon resonance (Table 1), with only G3-D showing an ~3-fold slower off-rate on cells. Because the on-rates of the G3 mutants on cells are very similar to each other, affinities on cells are directly determined by off-rates on cells.

The best binder, G3, has an affinity of ~60 to 100 pmol/L also on cells. The epitope on domain-4 of HER2, recognized by the G3-derived DARPins, may thus be better accessible than the one recognized by trastuzumab.

The bivalent DARPin G3-G3 shows a similar on-rate as the monovalent DARPins, but its off-rate is too small to be

Table 1. Affinities and kinetic parameters of anti-HER2 DARPins investigated

DARPin*	BT474 cells†			BIACORE‡		
	$k_{on}/10^5$ (mol/L)$^{-1}$ s^{-1}	$k_{off}/10^{-3}$ s^{-1}	K_D/(nmol/L)	$k_{on}/10^5$ (mol/L)$^{-1}$ s^{-1}	$k_{off}/10^{-3}$ s^{-1}	K_D/(nmol/L)
G3	10.3 ± 2.76	0.069 ± 0.02	0.070 ± 0.018	11.2 ± 0.02	0.102 ± 0.001	0.091 ± 0.001
G3-D	7.51 ± 0.57	0.22 ± 0.02	0.29 ± 0.3	7.68 ± 0.04	1.14 ± 0.002	1.48 ± 0.008
G3-AVD	3.96 ± 2.1	3.3 ± 1.5	10.2 ± 5.9	4.35 ± 0.02	4.42 ± 0.008	10.2 ± 0.055
G3-HAVD	nd	nd	nd	0.028 ± 0.01	0.739 ± 0.003	269 ± 1.19
G3-G3	10.0 ± 3.55	0.01	0.011 ± 0.004	2.8 ± 0.2	<0.001§	<0.01§

Abbreviation: nd, not determined.

*DARPins with mutations affecting the affinity and bivalent DARPin (see text).

†Association and dissociation kinetics were determined on BT474 cells by following the mean fluorescence intensity with fluorescence-activated cell sorting as a function of time, as shown in Supplementary Fig. S5. This table summarizes the data extracted from Supplementary Fig. S5. The error on cell binding rates reflects the differences between independent experiments, whereas the error on off-rates is the statistical error on fitting.

‡For comparison, the data previously obtained by surface plasmon resonance are shown as well (17). The error shown for the surface plasmon resonance measurements only reflects the statistical error upon data fitting.

§For bivalent binding, avidities are not constants but depend on coating density. Measurements by C. Gehringer and H.K. Binz (unpublished data).

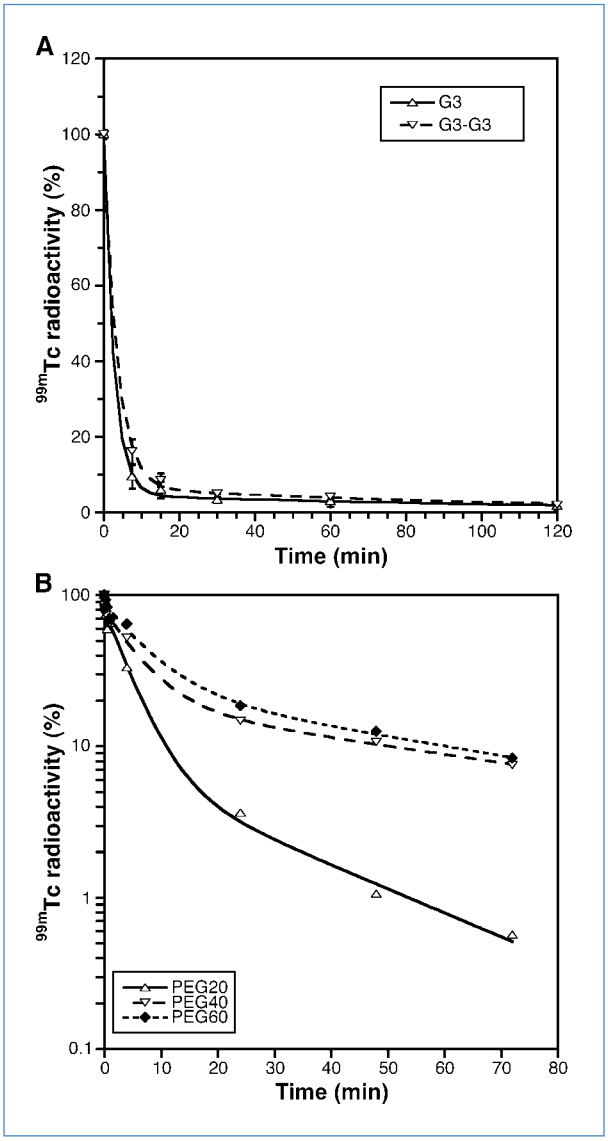

Figure 1. Clearance of different DARPin formats from serum in BALB/c mice not bearing a tumor. Samples of $^{99m}Tc(CO)_3$-labeled proteins were injected i.v. A, monovalent DARPin G3 and bivalent DARPin G3-G3; B, G3 DARPin derivatized with different PEG molecules.

measured ($<1 \times 10^{-6}$ s^{-1}; Supplementary Fig. S5), which directly shows bivalent binding on cells. As a control, we also measured G3-E2_5 (data not shown), and its dissociation rate matches that of G3, as expected from its single HER2-binding site.

Blood clearance in healthy BALB/c mice. For the unmodified DARPin G3, at 7.5 minutes, 90% of the radioactivity had already disappeared from the blood (Fig. 1A), suggesting a half-life of <3 minutes in which both tissue distribution and clearance through the kidney occurs. There may be an additional slow phase with only 5% amplitude and a half-life of 80 to 90 minutes (Fig. 1A). The bivalent DARPins are cleared almost as rapidly as well (Fig. 1A), suggesting, to a large extent, first-pass clearance for these small DARPins.

The serum clearance of PEGylated DARPins shows two slow phases. The initial phase (~1 day) might suggest a tissue distribution phase, before the even slower terminal plasma elimination (Fig. 1B; Supplementary Tables ST4 and ST5). The slowest phase correlates with the size of the PEG molecule (PEG20, ~19 hours; PEG40 and PEG60, ~50 hours). Therefore, as with many other PEGylated proteins, the terminal half-life is mostly determined by the hydrodynamics of the PEG molecule, preventing glomerular filtration and reducing the apparent volume of distribution at early times (see Discussion).

Tumor localization of unmodified DARPins. The targeting properties of the various constructs were examined in nude mice xenografted with human ovarian carcinoma SK-OV-3.ip cells, subcutaneously injected at the lateral flanks. Control experiments showed no significant differences with SK-OV-3 tumors (Supplementary Table ST1).

We first compared the biodistribution of 14.5 kDa DARPins after 1, 4, 24, and 48 hours (Fig. 2A, Table 2). Their half-life was very short, consistent with the measurements in BALB/c mice with shorter time points (Fig. 1A). Nonetheless, high tumor localization values were observed, ~8% ID/g for the construct with the highest affinity after 4 hours. Even after 48 hours, this value was still ~6.5% ID/g.

Because of the very low blood levels even after only 4 hours, very high tumor-to-blood values were reached (30 after 4 hours, >60 at 24 hours and beyond). The tissue distribution of the unmodified DARPin G3 was measured in eight different experimental series, all falling within 1 SD from the mean (Fig. 2A).

For the other unmodified DARPins with lower affinity (Table 1), tumor accumulation was lower, and proportional to affinity (Fig. 2A; Table 2). There was no indication of a leveling-off at high affinity, an effect which has been observed with bigger targeting reagents (refs. 11, 12; see Discussion).

The control DARPin E3_5 (20) with no affinity to HER2 was also tested (Fig. 2C; Supplementary Table ST1), and after 24 hours, only 0.46% ID/g was located at the tumor, showing that localization depends on specific binding to HER2.

Tumor localization of DARPin-linker-DARPin constructs. Both the bivalent G3-G3 construct, and a monovalent G3-E2_5 construct, in which the second DARPin had no affinity with HER2, were investigated. In both cases, the amount observed at the tumor was lower than for the monovalent G3 (Fig. 2C; time course in Supplementary Table ST2). Because G3-G3 and G3-E2_5 show essentially the same tumor uptake (Supplementary Table ST2), the higher avidity of G3-G3 seems to neither contribute to additional tumor retention nor could an additional barrier effect explain the lower tumor accumulation. Instead, we propose this lower accumulation to be an effect of the higher molecular weight (see Discussion).

Tumor localization of PEGylated DARPins. Cys-containing derivatives were made, giving equally high yields in production as their parent molecules, and coupling of PEG20 was almost quantitative. Tumor accumulation for G3-PEG20 after 24 hours reaches 13.4% ID/g (Fig. 2B; Table 2; Supplementary Table ST3) and shows much slower tumor accumulation.

Tumor values stay very high throughout the experiment (Supplementary Tables ST3 and ST6). This slow accumulation suggests that the protein in the blood acts as a reservoir from which slow extravasation to the tumor occurs over a long duration. The slow off-rates from HER2 allow a slow but steady build-up.

The second difference to the non-PEGylated proteins is that tumor accumulation seems to depend less on affinity than for the non-PEGylated DARPins (Fig. 2B). Only the lowest-affinity binder (K_D = 270 nmol/L) is just slightly above the background of a nonbinding control (see above), illustrating that tumor enrichment is dependent on specific binding to HER2. Due to the slower blood clearance, the tumor-to-blood ratios at early times are much smaller, and the highest values (~20) are only reached after 72 hours (Supplementary Table ST6).

We also compared the tumor accumulation of DARPin G3, coupled to PEG20 and PEG60 (Supplementary Table ST3). The PEG60 construct seemed to be retained slightly more at the tumor site after 48 hours, suggesting a role of the serum reservoir in an extended tumor loading phase.

Organ distribution. The distribution to liver and kidney gives information about the preferred elimination pathway of the DARPins. As expected, the small DARPins are eliminated predominantly via the kidney. $^{99m}Tc(CO)_3$ is a residualizing labeling reagent which remains in the kidney cells following endocytosis (31, 32) due to the high stability of the ^{99m}Tc label at the His-tag of the proteins (27) and the inability of the cell to excrete this label. High kidney values are observed for all monovalent DARPins (Table 2), as for scFv fragments (27, 31, 32) and camel VHH domains (33). For the constructs with two linked DARPins, predominant elimination via the kidney is seen as well, but the values are somewhat lower and the liver values correspondingly slightly higher (Supplementary Table ST2), even though this is not reflected in a significantly longer serum half-life.

The PEGylated proteins gave rise to a much lower percentage of label found in the kidney (Table 2). As expected from similar studies with PEGylated antibody fragments (10, 26), PEGylated DARPins are thus eliminated to a greater extent via the liver.

Organ distribution in healthy BALB/c mice. After 24 hours, similar values for kidney accumulation and only low liver accumulation were found as in tumor-bearing nude

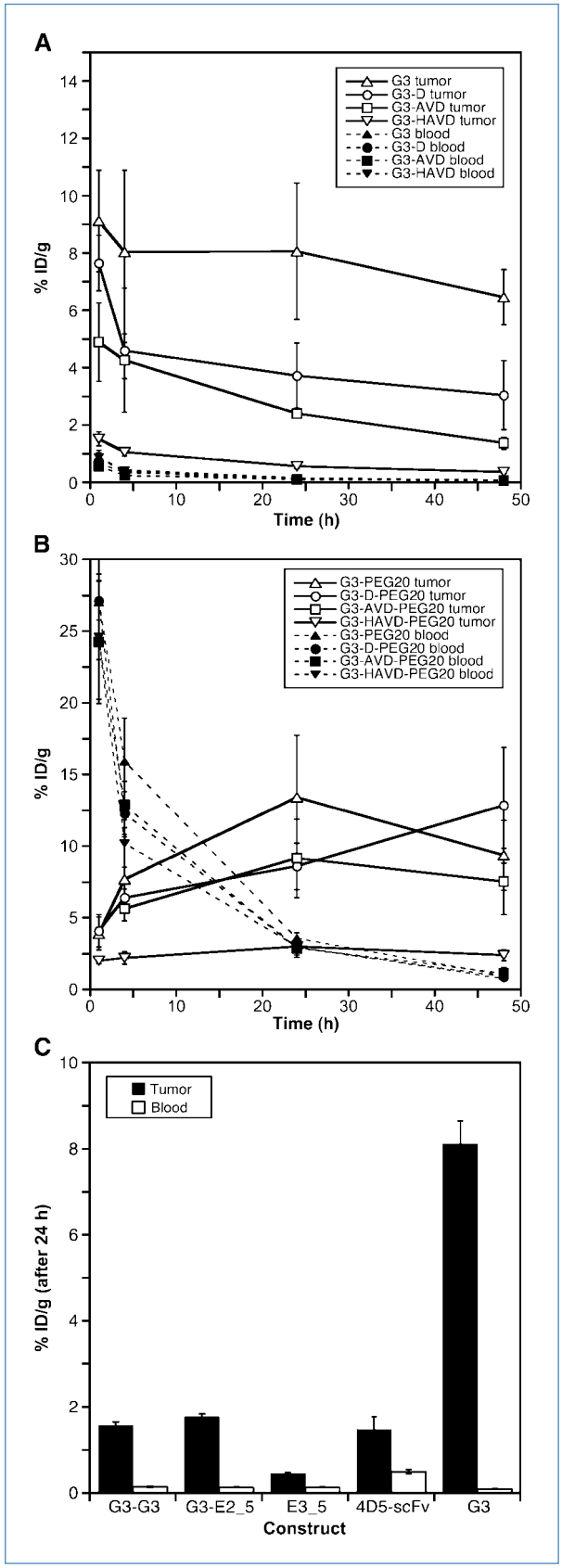

Figure 2. Time-dependent changes in organ distribution of DARPins of different affinity (see Table 1) without (A) and with (B) derivatization with PEG20. The mean % ID/g tissue (±SD) at each time point are given for tumor and blood (for detailed data, see Table 2). Samples of $^{99m}Tc(CO)_3$-labeled proteins were injected i.v. into nude mice bearing SK-OV-3.ip carcinoma xenografts. Mice (n = 3 per time point) were sacrificed at the times indicated after injection, organs were excised, and the incorporated radioactivity was determined. C, different DARPin formats and controls after 24 h (additional time course and organ distribution data in Supplementary Tables ST1 and ST2). G3-G3, bivalent HER2-binding DARPin; G3-E2_5, HER2-binding DARPin fused to a nonselected DARPin without affinity for HER2; E3_5, nonselected DARPin without affinity for HER2; 4D5 scFv, anti-HER2 single-chain Fv fragment; G3, monovalent HER2-binding DARPin (Table 1).

Table 2. Tissue distributions of DARPins in SK-OV-3.ip tumor bearing mice

	Unmodified DARPins					PEG20 modified DARPins			
Organ	**1 h**	**4 h**	**24 h**	**48 h**	**Organ**	**1 h**	**4 h**	**24 h**	**48 h**
G3					G3-PEG20				
Blood	0.72 ± 0.05	0.30 ± 0.06	0.13 ± 0.02	0.09 ± 0.02	Blood	25.41 ± 3.94	13.45 ± 2.83	2.83 ± 0.96	0.87 ± 0.13
Heart	0.90 ± 0.03	0.51 ± 0.10	0.32 ± 0.04	0.27 ± 0.05	Heart	8.70 ± 2.22	4.93 ± 1.32	1.43 ± 0.50	0.88 ± 0.15
Lung	1.79 ± 0.14	0.70 ± 0.12	0.38 ± 0.06	0.34 ± 0.09	Lung	10.98 ± 2.56	6.55 ± 2.03	1.92 ± 0.60	0.96 ± 0.25
Spleen	2.05 ± 0.19	1.79 ± 0.61	0.96 ± 0.21	0.98 ± 0.18	Spleen	5.50 ± 1.69	3.47 ± 0.85	2.61 ± 1.05	1.91 ± 0.88
Kidney	267.75 ± 29.44	239.49 ± 32.85	145.65 ± 19.49	110.66 ± 31.84	Kidney	24.08 ± 3.72	34.59 ± 7.48	36.78 ± 13.90	28.75 ± 9.68
Stomach	1.33 ± 0.10	0.62 ± 0.17	0.59 ± 0.30	0.34 ± 0.11	Stomach	2.72 ± 0.73	2.18 ± 0.61	0.95 ± 0.30	0.57 ± 0.21
Colon	0.85 ± 0.25	0.45 ± 0.10	0.43 ± 0.16	0.24 ± 0.05	Colon	3.42 ± 0.56	2.06 ± 0.42	0.87 ± 0.20	0.48 ± 0.24
Liver	7.96 ± 0.55	7.27 ± 1.04	4.61 ± 0.59	3.78 ± 0.91	Liver	9.82 ± 1.97	8.97 ± 2.42	7.14 ± 2.26	5.17 ± 1.71
Muscle	0.48 ± 0.06	0.27 ± 0.03	0.17 ± 0.03	0.15 ± 0.03	Muscle	0.97 ± 0.14	0.98 ± 0.13	0.63 ± 0.14	0.44 ± 0.07
Bone	1.61 ± 0.22	1.11 ± 0.05	0.81 ± 0.15	0.79 ± 0.21	Bone	2.71 ± 0.89	1.88 ± 0.42	1.02 ± 0.27	0.71 ± 0.19
Tumor	9.12 ± 1.77	8.04 ± 2.85	8.06 ± 2.38	6.46 ± 0.96	Tumor	3.90 ± 1.14	7.70 ± 2.93	13.42 ± 4.29	9.37 ± 2.44
T:B	12.67 ± 3.34	26.80 ± 14.86	62.00 ± 27.85	71.78 ± 26.62	T:B	0.15 ± 0.07	0.57 ± 0.34	4.73 ± 3.12	10.77 ± 4.37
G3-D					G3-D-PEG20				
Blood	0.67 ± 0.10	0.34 ± 0.11	0.13 ± 0.04	0.06 ± 0.01	Blood	24.24 ± 4.27	12.90 ± 1.61	2.89 ± 0.50	1.14 ± 0.37
Heart	0.58 ± 0.09	0.41 ± 0.14	0.20 ± 0.02	0.14 ± 0.02	Heart	7.55 ± 1.80	4.68 ± 0.34	1.79 ± 0.28	1.01 ± 0.26
Lung	1.12 ± 0.33	0.53 ± 0.13	0.14 ± 0.20	0.20 ± 0.06	Lung	12.00 ± 2.43	6.60 ± 0.54	1.88 ± 0.36	1.07 ± 0.30
Spleen	1.10 ± 0.11	0.88 ± 0.05	0.56 ± 0.06	0.35 ± 0.11	Spleen	5.23 ± 1.41	4.47 ± 0.79	2.73 ± 0.74	2.78 ± 0.62
Kidney	195.00 ± 10.49	155.99 ± 37.08	91.82 ± 6.05	66.09 ± 9.28	Kidney	20.34 ± 44.11	29.85 ± 23.18	46.42 ± 5.34	33.75 ± 0.25
Stomach	0.85 ± 0.28	0.41 ± 0.03	0.15 ± 0.12	0.20 ± 0.08	Stomach	3.05 ± 1.75	2.29 ± 0.08	0.74 ± 0.06	0.41 ± 0.23
Colon	0.52 ± 0.06	0.45 ± 0.09	0.22 ± 0.06	0.13 ± 0.02	Colon	3.12 ± 1.51	1.98 ± 0.16	0.84 ± 0.16	0.63 ± 0.12
Liver	4.74 ± 0.88	4.45 ± 1.18	2.45 ± 0.31	1.76 ± 0.23	Liver	11.60 ± 2.29	10.05 ± 1.17	7.38 ± 1.95	6.82 ± 0.20
Muscle	0.32 ± 0.02	0.22 ± 0.06	0.11 ± 0.02	0.07 ± 0.01	Muscle	0.88 ± 0.06	0.91 ± 0.08	0.57 ± 0.11	0.53 ± 0.11
Bone	0.94 ± 0.01	0.54 ± 0.01	0.29 ± 0.08	0.36 ± 0.02	Bone	2.43 ± 0.44	1.67 ± 0.13	0.96 ± 0.29	0.98 ± 0.32
Tumor	7.65 ± 0.97	4.61 ± 2.17	3.73 ± 1.13	3.05 ± 1.20	Tumor	4.09 ± 1.13	6.39 ± 0.61	8.59 ± 1.61	12.85 ± 4.03
T:B	11.42 ± 3.15	13.56 ± 10.77	28.69 ± 17.52	50.83 ± 28.47	T:B	0.17 ± 0.08	0.50 ± 0.11	2.97 ± 1.07	11.30 ± 7.27
G3-AVD					G3-AVD-PEG20				
Blood	0.57 ± 0.00	0.25 ± 0.03	0.10 ± 0.01	0.06 ± 0.01	Blood		14.31 ± 1.87	3.75 ± 0.87	0.93 ± 0.35
Heart	0.60 ± 0.05	0.40 ± 0.07	0.23 ± 0.02	0.18 ± 0.03	Heart		6.14 ± 0.23	2.25 ± 0.72	0.89 ± 0.21
Lung	0.87 ± 0.08	0.37 ± 0.31	0.31 ± 0.04	0.19 ± 0.04	Lung		7.21 ± 1.08	2.63 ± 0.62	0.99 ± 0.30
Spleen	1.64 ± 0.13	1.40 ± 0.26	0.87 ± 0.05	0.87 ± 0.13	Spleen		4.68 ± 1.25	4.92 ± 1.69	2.88 ± 1.03
Kidney	195.57 ± 7.85	163.00 ± 27.65	89.35 ± 12.12	58.22 ± 10.53	Kidney		46.26 ± 7.33	74.08 ± 9.46	40.42 ± 4.92
Stomach	0.89 ± 0.27	0.55 ± 0.18	0.23 ± 0.01	0.15 ± 0.06	Stomach		2.58 ± 0.67	1.07 ± 0.39	0.64 ± 0.07
Colon	0.59 ± 0.06	0.50 ± 0.16	0.28 ± 0.03	0.15 ± 0.02	Colon		2.13 ± 0.04	1.29 ± 0.25	0.56 ± 0.06
Liver	6.84 ± 0.80	6.13 ± 1.13	3.65 ± 0.84	2.22 ± 0.08	Liver		12.92 ± 2.14	11.68 ± 1.31	8.13 ± 1.97
Muscle	0.33 ± 0.03	0.24 ± 0.02	0.13 ± 0.02	0.09 ± 0.08	Muscle		0.96 ± 0.14	0.80 ± 0.28	0.41 ± 0.13
Bone	0.99 ± 0.12	0.76 ± 0.16	0.46 ± 0.02	0.39 ± 0.08	Bone		2.22 ± 0.33	1.82 ± 0.39	1.19 ± 0.60
Tumor	4.90 ± 1.37	4.26 ± 0.63	2.41 ± 0.17	1.38 ± 0.21	Tumor		5.66 ± 0.85	9.15 ± 2.73	7.51 ± 2.32
T:B	8.60 ± 2.45	17.04 ± 4.56	24.10 ± 4.11	23.00 ± 7.33	T:B		0.40 ± 0.11	2.44 ± 1.30	8.07 ± 5.51
G3-HAVD					G3-HAVD-PEG20				
Blood	0.89 ± 0.16	0.43 ± 0.04	0.15 ± 0.03	0.09 ± 0.10	Blood	24.60 ± 4.35	10.19 ± 1.66	3.02 ± 0.31	0.75 ± 0.10
Heart	0.95 ± 0.16	0.59 ± 0.07	0.32 ± 0.06	0.22 ± 0.04	Heart	7.57 ± 1.92	3.06 ± 0.60	1.59 ± 0.09	0.75 ± 0.09
Lung	1.30 ± 0.10	0.81 ± 0.23	0.35 ± 0.03	0.25 ± 0.02	Lung	10.89 ± 1.77	4.56 ± 0.63	2.14 ± 0.06	0.82 ± 0.08

(*Continued on the following page*)

Table 2. Tissue distributions of DARPins in SK-OV-3.ip tumor bearing mice (Cont'd)

	Unmodified DARPins					PEG20 modified DARPins			
Organ	1 h	4 h	24 h	48 h	Organ	1 h	4 h	24 h	48 h
Spleen	1.90 ± 0.16	1.57 ± 0.13	0.95 ± 0.28	0.83 ± 0.12	Spleen	6.01 ± 1.07	2.54 ± 0.31	3.46 ± 0.39	2.57 ± 0.04
Kidney	203.38 ± 34.96	162.01 ± 21.66	93.48 ± 13.81	69.26 ± 15.93	Kidney	16.04 ± 2.78	11.62 ± 1.64	18.93 ± 2.90	13.07 ± 1.20
Stomach	0.92 ± 0.09	0.71 ± 0.09	0.28 ± 0.27	0.17 ± 0.06	Stomach	2.88 ± 0.58	1.47 ± 0.25	1.03 ± 0.38	0.60 ± 0.06
Colon	0.81 ± 0.11	0.66 ± 0.02	0.32 ± 0.02	0.15 ± 0.01	Colon	3.18 ± 0.67	1.56 ± 0.01	1.03 ± 0.09	0.46 ± 0.03
Liver	8.68 ± 0.91	7.05 ± 0.67	3.93 ± 1.09	2.98 ± 0.50	Liver	9.46 ± 1.79	6.01 ± 0.94	7.28 ± 1.38	4.67 ± 0.18
Muscle	0.44 ± 0.06	0.28 ± 0.06	0.17 ± 0.02	0.10 ± 0.01	Muscle	0.84 ± 0.18	0.56 ± 0.16	0.66 ± 0.33	0.38 ± 0.02
Bone	1.44 ± 0.37	0.96 ± 0.11	0.64 ± 0.09	0.50 ± 0.03	Bone	2.80 ± 0.41	1.46 ± 0.10	1.21 ± 0.32	0.71 ± 0.09
Tumor	1.52 ± 0.24	1.07 ± 0.15	0.57 ± 0.08	0.36 ± 0.06	Tumor	2.01 ± 0.21	2.21 ± 0.43	3.01 ± 0.32	2.39 ± 0.38
T:B	1.71 ± 0.58	2.49 ± 0.58	3.80 ± 1.29	4.00 ± 4.89	T:B	0.08 ± 0.02	0.22 ± 0.08	1.00 ± 0.21	3.19 ± 0.91

NOTE: Biodistributions of unmodified and PEGylated DARPins and with different affinity were analyzed in nude mice, xenografted with human ovarian carcinoma SK-OV-3.ip tumors. Mice (n = 3 per time point) were sacrificed and organs excised at the times indicated after injection of the $^{99m}Tc(CO)_3$-labeled constructs. Data are given as the percentage of injected dose per gram of tissue (% ID/g) and expressed as the mean ± SD.

mice (Supplementary Tables ST4–ST5). The same correspondence between BALB/c mice and tumor-bearing nude mice was found for the biodistribution of G3-PEG20 derivatives, showing that the nude mice phenotype has no influence on the biodistribution of DARPins.

Imaging the distribution of radioactivity within the tumor. We investigated the penetration of the highest affinity DARPin G3 by imaging slices of a SK-OV-3.ip tumor 24 hours after injection, using both X-ray film (Fig. 3A and B) and a Packard InstantImager (Fig. 3C and D). Clearly, the protein penetrates the whole tumor mass quite evenly, with a potentially slightly stronger staining near the rim of the tumor, which might have been expected for high-affinity molecules (see Discussion).

SPECT/CT imaging studies. A whole-body SPECT/CT of a mouse bearing tumors left and right of the shoulders was performed with $^{99m}Tc(CO)_3$-labeled G3 (Fig. 4A) 24 hours after i.v. injection and compared with a scan of a mouse injected with $^{99m}Tc(CO)_3$-labeled G3-PEG20 (Fig. 4B). For both DARPins, high accumulation of radioactivity was detected in tumors localized on both shoulders. Significantly less accumulation of radioactivity was found in the kidneys of the mouse injected with the PEGylated DARPin.

A high-resolution SPECT/CT image (Fig. 4C) of a SK-OV-3.ip tumor on the right hind leg, 24 hours after targeting with DARPin G3, showed accumulation of the radioactivity in the tumor with some preferential detection at the rim. Because the field of view in this study is reduced to 30 × 30 mm, the nonspecific accumulation in nontargeted organs such as the kidney is not visible.

Discussion

The four goals of this study were to (*a*) quantitatively test the ability of DARPins to target to tumors in mice, (*b*) examine the optimal DARPin tumor targeting format, (*c*) evaluate the dependence of targeting on DARPin affinity, and (*d*) examine the relationship between size, valency, and affinities for the most effective tumor targeting, and to derive general principles for targeting molecules by comparing the results with other reports on targeting HER2.

We will argue in the following that the favorable uptake values of unmodified DARPins are a combination of high affinity and small size, which allows efficient extravasation and retention at the tumor. These targeting properties also capitalize on the lack of aggregation of DARPins (refs. 19, 21, 34; Supplementary Figs. S7–S10). Biophysical stability has been previously shown to directly improve tumor targeting (35).

Higher tumor accumulation values can be reached by IgGs by virtue of their FcRn-mediated long serum half-life (36), but with a correspondingly long tissue half-life and more limited tumor penetration.

Influence of affinities on unmodified DARPins. The total amount located at the tumor is directly proportional to affinity, and there is no leveling off with affinity (Fig. 2A). This was found over the whole time range measured. The serum half-life seems to be, as expected, comparable for the DARPin point mutants investigated, and thus these higher tumor enrichments also parallel higher tumor-to-blood ratios, proportional to affinity. Because the on-rates are very similar among the DARPins, both on cells and on pure proteins (Table 1; except for the binder with the lowest affinity; ref. 24), total build-up and retention at the tumor seems to be governed by the dissociation rates from the target.

DARPin constructs with additional domains. The bivalent molecule did not show improved targeting over the monomeric one, but instead lower accumulation, despite its extremely slow off-rate, in turn demonstrating that binding

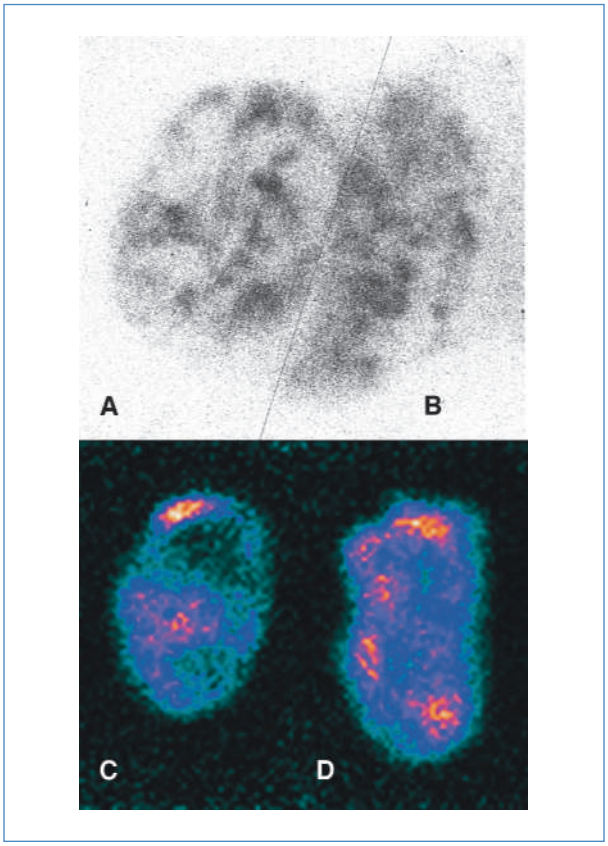

Figure 3. *Ex vivo* autoradiogram of SK-OV-3.ip tumor slices imaged with $^{99m}Tc(CO)_3$-labeled DARPin G3, 24 h after i.v. injection. The slices were put on Kodak X-Omat Blue film and exposed for 4 h (A, rim; B, middle section). The radioactivity was also recorded with a Packard InstantImager (C, rim; D, middle section).

on cells is really bivalent. Tumor accumulation was equally low for a two-domain DARPin with only one functional site. This suggests that the lower accumulation was governed by molecular size, and not by a barrier effect of this high-avidity construct. For both DARPin-DARPin fusions (molecular weight, 30 kDa), tumor accumulations (<2% ID/g) were very similar to those of monovalent anti-HER2 scFv fragments (molecular weight 25 kDa) with affinities on cells of 1 to 320 nmol/L in similar SK-OV-3 models (9, 10, 26, 37, 38).

The influence of PEGylation. The depot function of the PEGylated molecules in serum, evidenced by their prolonged terminal half-life (~19 hours), probably coupled with slow extravasation and diffusion, leads to a slower build-up on the tumor, and limits the achievable tumor-to-blood ratios.

The importance of affinity for the extent of tumor accumulation is diminished for the PEGylated constructs, compared with the underivatized constructs. Similarly, for whole antibodies, affinity did not seem to increase total tumor accumulation above a certain threshold affinity (11).

A pure physical effect has been proposed to contribute to the tumor uptake of large macromolecules and nanoparticles, termed enhanced permeability and retention (39, 40). However, because the PEGylated variant with K_D = 270 nmol/L (Fig. 2B) showed almost no tumor accumulation, we can conclude that specific binding with reasonable affinity is essential and the enhanced permeability and retention effect is insignificant.

PEGylated monomeric and dimeric scFv constructs showed similar tumor accumulation (26) as PEGylated DARPins, and thus, it is largely determined by hydrodynamic properties of the PEG. However, because of their robustness and the unique cysteine, PEGylated DARPins are easier to prepare.

Comparison to antibody scFv fragments. We restrict our discussion to targeting studies of HER2 in SK-OV-3 tumors, and where the affinity *on cells* has been measured, because to pure antigen, it is potentially different (28–30). With the scFv 4D5 (refs. 10, 26; K_D = 9–29 nmol/L on cells), tumor accumulations of 1% to 1.77% ID/g were obtained after 24 hours.

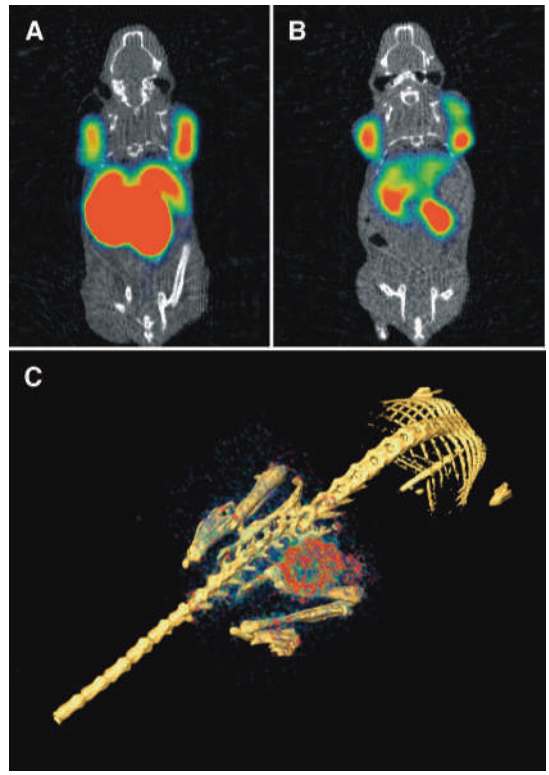

Figure 4. Whole body SPECT/CT (low resolution, high sensitivity) scans after i.v. injection of labeled DARPins. A, coronal section of a mouse with two SK-OV-3.ip tumors on both shoulders injected with $^{99m}Tc(CO)_3$-labeled DARPin G3. Mouse A (G3; whole body activity of 18.5 MBq) was scanned after 22 h with an acquisition time of 32 min. B, mouse with two SK-OV-3.ip tumors on both shoulders injected with $^{99m}Tc(CO)_3$-labeled DARPin G3-PEG20. C, three-dimensional SPECT/CT (high resolution, low sensitivity, pinhole collimator) scan of a SK-OV-3.ip tumor located at the right hind leg 24 h after i.v. injection with $^{99m}Tc(CO)_3$-labeled DARPin G3 with an acquisition time of 4 h. In all experiments, the same dose of radioactivity was injected (555 MBq).

The scFv C6.5 (K_D = 70 nmol/L on cells) was evolved to K_D = 3.8 nmol/L, however, only marginally changing tumor accumulation from 1.32% to 1.42% ID/g (41), or from 0.80% to 1.48% ID/g (38). The nanomolar K_D of these monovalent scFv on cells, compared with the picomolar DARPin, might contribute to the lower accumulation observed.

scFv fragments have been converted to bivalent and tetravalent miniantibodies by fusing self-assembling peptides to the COOH terminus (10, 26), but tumor accumulation was only moderately increased to 2.84% ID/g for the tetramer. A 135 kDa trivalent molecule, made via barnase-barstar fusions and being above the renal filtration threshold, showed a higher increase (7.04% ID/g; ref. 42) and a longer terminal half-life.

When the scFv fragment C6.5 and its high-affinity derivative were converted to diabodies (functional affinity on cells 3.4 and 0.49 nmol/L, respectively), 6.48% and 3.18% ID/g were reported. Note that the higher avidity molecule performed worse (41). The evolved monovalent C6.5 scFv (K_D = 3.8 nmol/L on cells) only lead to 1.42% ID/g on the tumor. Size does not seem to be the crucial difference, however, because a monovalent scFv and the corresponding diabody with only one functional site showed the same tumor accumulation (37). A more efficient internalization of the particular bivalent diabody might lead to a better retention of label, even at a similar functional affinity.

In mice with kidneys removed (12, 38), tumor accumulation of all fragments was increased. In this artificial model, no further increase in tumor accumulation was found beyond a functional affinity of $\sim 10^{-9}$ mol/L, with even a drop for one data point at 10^{-11} mol/L. The high-affinity molecules predominantly localized at the periphery of the tumor, whereas the low-affinity molecules—at the same total dose—localized diffusely throughout the tumor.

This peripheral location is consistent with the "shrinking core model" (8, 43), in which antigens are occupied starting from the tumor outside and progressing to the inside. Every antigen encountered is occupied and remains so, if the off-rate is low, whereas the molecules dissociate and transiently rebind further inward (but also leave the tumor), if the off-rate is faster. This concept has been originally proposed for whole antibodies in similar form (11).

Taken together, these studies with scFv monomers and multimers have found increased tumor accumulation with increasing valency, and in some cases, functional affinity. The extent, however, varied significantly between constructs. Higher molecular weight is favorable only if it brings the molecule above the renal filtration threshold by increasing the terminal half-life. Nonetheless, the data have also suggested that an increase in functional affinity beyond a certain threshold is not useful for molecules the size of an scFv and its multimers. We show here that some of these limitations are not found for smaller high-affinity molecules such as DARPins.

Comparison to other scaffolds targeting HER2. Affibodies and other small scaffolds have also been selected to bind to HER2 (44), and one such molecule with K_D = 50 nmol/L has been affinity-matured to 22 pmol/L (measured on purified HER2). To our knowledge, the affinity on whole cells has not been reported. The evolved affibody showed tumor uptakes reaching 8.6% ID/g after 24 hours (45).

The original monovalent affibody (K_D = 50 nmol/L) was also made bivalent (functional affinity ~3 nmol/L), but bivalent binding on cells was not tested. The tumor uptake was 2.6% ID/g after 12 hours (46), significantly less than for the evolved monomer, with the caveat that the labeling method was not always the same.

Tumor localization of single-domain antibodies directed against HER2 has not been reported. Two camel VHH domains, specific for epidermal growth factor receptor (K_D = 2.3 and 5.7 nmol/L *in vitro*), were reported with tumor uptakes of 9.1% ID/g and 6.1% ID/g, measured 1.5 hours after injection (33).

Taken together, these results support our hypothesis that predicts favorable targeting properties for molecules which combine high affinity with small molecular size.

The importance of molecular weight. The molecular weight influences at least three parameters critical for targeting (*a*) capillary extravasation, (*b*) diffusion, and (*c*) renal clearance (8, 36).

There may be a rather steep dependence of tumor vascular permeability on molecular weight (47), with smaller molecules showing significantly greater permeability, even in tumor capillaries. This has been well known for normal capillaries (48). For proteins with a Stokes-Einstein radius of 40 Å, only very low levels are found outside the plasma, whereas proteins of 20 Å almost completely equilibrate with interstitial fluid or lymph. DARPins would probably behave like the latter (49), and because of the measured steep molecular weight dependence, have significantly higher permeability than scFv fragments and other larger constructs. In earlier work, permeability varied only 2-fold for substances between 25 and 160 kDa (scFv to full IgG; ref. 50), but recent work suggests much stronger trends when extending studies to smaller molecular weights (47). The capillary permeability may be the limiting parameter controlling the flow of antibodies reaching the tumor (8).

Because of the lack of lymphatic drainage in a tumor, proteins are moving from the capillary to the tumor center by diffusion, with negligible convection (8). The diffusion coefficient of an scFv and a PEGylated scFv differs only by a factor of 2 (28), and the differences between DARPin and scFv would be smaller still. Nonetheless, hindered diffusion through tumor interstitial space might augment this difference.

The underivatized DARPins are cleared through the kidney, giving rise to a rather short serum half-life and an observable accumulation of radioactivity in the kidney, very similar to scFv fragments or camelid VHH domains (see above).

An increase in molecular weight seems to be beneficial for tumor uptake only once the molecule is brought above the renal filtration cutoff (42). The addition of a nonfunctional binding site is neither beneficial for scFvs (37) nor DARPins (see above).

There are two modes of efficient targeting. Our conclusions are consistent with a mathematical model (36) published after the submission of this article. First, DARPins and presumably other small, very soluble proteins with picomolar affinity, also show high tumor accumulation with very fast clearance through the liver and kidney. This is probably due to high extravasation and tumor penetration, and requires a very slow off-rate from the target, leading to efficient tumor retention. Targeting is proportional to affinity and no plateau with affinity was seen, suggesting that still higher affinities might further increase tumor targeting.

Second, very large proteins such as monoclonal antibodies or PEGylated DARPins achieve even higher tumor loads due the long circulation and (slow) equilibration with the tumor, but the elimination from blood and nontumor tissue is also slow, and tumor-to-tissue ratios remain lower.

Intermediate size molecules (fused DARPins, scFv fragments) show lower tumor accumulation because elimination through the kidney is equally rapid, but extravasation, and perhaps tumor diffusion, is diminished. The very tight binding of a bivalent DARPin does not compensate this effect.

Disclosure of Potential Conflicts of Interest

C. Zahnd, M. Kawe, M.T. Stumpp, H.K. Binz, and A. Plückthun are shareholders of Molecular Partners AG, which is commercializing the DARPin technology.

Acknowledgments

We thank Christian Gehringer and Frank Zoller for help in plasmid constructions, Martin Schwill for help in the fluorescence labeling, as well as Dr. Patrik Forrer, Dr. Patrick Amstutz, and Prof. Dr. Uwe Zangemeister-Wittke for helpful discussions. The DARPin technology is commercialized by Molecular Partners AG, Wagistrasse 14, 8952 Schlieren, Switzerland (http://www.molecularpartners.com).

Grant Support

Kommission für Technologie und Innovation, Gebert-Rüf-Stiftung (GRS-054/04; M.T. Stumpp), Swiss Cancer League (Krebsliga Schweiz; KLS-01686-02-2005), Oncosuisse (OCS-02128-08-2007), and University of Zurich.

The costs of publication of this article were defrayed in part by the payment of page charges. This article must therefore be hereby marked *advertisement* in accordance with 18 U.S.C. Section 1734 solely to indicate this fact.

Received 9/14/09; revised 11/20/09; accepted 12/9/09; published OnlineFirst 2/2/10.

References

1. Waldmann TA, Morris JC. Development of antibodies and chimeric molecules for cancer immunotherapy. Adv Immunol 2006;90:83–131.
2. Dalle S, Thieblemont C, Thomas L, Dumontet C. Monoclonal antibodies in clinical oncology. Curr Med Chem Anticancer Agents 2008;8:523–32.
3. Boyiadzis M, Foon KA. Approved monoclonal antibodies for cancer therapy. Expert Opin Biol Ther 2008;8:1151–8.
4. Moroney SE, Plückthun A. Modern antibody technology: the impact on drug development. In: Knäblein J, editor. Modern biopharmaceuticals. Weinheim: Wiley-VCH; 2005, p. 1147–86.
5. Cobleigh MA, Vogel CL, Tripathy D, et al. Multinational study of the efficacy and safety of humanized anti-HER2 monoclonal antibody in women who have HER2-overexpressing metastatic breast cancer that has progressed after chemotherapy for metastatic disease. J Clin Oncol 1999;17:2639–48.
6. Nahta R, Esteva FJ. Herceptin: mechanisms of action and resistance. Cancer Lett 2006;232:123–38.
7. Carter PJ, Senter PD. Antibody-drug conjugates for cancer therapy. Cancer J 2008;14:154–69.
8. Thurber GM, Schmidt MM, Wittrup KD. Antibody tumor penetration: transport opposed by systemic and antigen-mediated clearance. Adv Drug Deliv Rev 2008;60:1421–34.
9. Adams GP, McCartney JE, Tai MS, et al. Highly specific *in vivo* tumor targeting by monovalent and divalent forms of 741F8 anti-c-erbB-2 single-chain Fv. Cancer Res 1993;53:4026–34.
10. Willuda J, Kubetzko S, Waibel R, Schubiger PA, Zangemeister-Wittke U, Plückthun A. Tumor targeting of mono-, di- and tetravalent anti-p185HER-2 miniantibodies multimerized by self-associating peptides. J Biol Chem 2001;276:14385–92.
11. Fujimori K, Covell DG, Fletcher JE, Weinstein JN. A modeling analysis of monoclonal antibody percolation through tumors: a binding-site barrier. J Nucl Med 1990;31:1191–8.
12. Adams GP, Schier R, McCall AM, et al. High affinity restricts the localization and tumor penetration of single-chain Fv antibody molecules. Cancer Res 2001;61:4750–5.
13. Ross JS, Fletcher JA. The HER-2/neu oncogene in breast cancer: prognostic factor, predictive factor, and target for therapy. Oncologist 1998;3:237–52.
14. Slamon DJ, Godolphin W, Jones LA, et al. Studies of the HER-2/neu proto-oncogene in human breast and ovarian cancer. Science 1989;244:707–12.
15. Holbro T, Hynes NE. ErbB receptors: directing key signaling networks throughout life. Annu Rev Pharmacol Toxicol 2004;44:195–217.
16. Yarden Y, Sliwkowski MX. Untangling the ErbB signalling network. Nat Rev Mol Cell Biol 2001;2:127–37.
17. Cho HS, Mason K, Ramyar KX, et al. Structure of the extracellular region of HER2 alone and in complex with the Herceptin Fab. Nature 2003;421:756–60.
18. Lee-Hoeflich ST, Crocker L, Yao E, et al. A central role for HER3 in HER2-amplified breast cancer: implications for targeted therapy. Cancer Res 2008;68:5878–87.
19. Binz HK, Amstutz P, Kohl A, et al. High-affinity binders selected from designed ankyrin repeat protein libraries. Nat Biotechnol 2004;22:575–82.
20. Binz HK, Stumpp MT, Forrer P, Amstutz P, Plückthun A. Designing repeat proteins: well-expressed, soluble and stable proteins from combinatorial libraries of consensus ankyrin repeat proteins. J Mol Biol 2003;332:489–503.
21. Wetzel SK, Settanni G, Kenig M, Binz HK, Plückthun A. Folding and unfolding mechanism of highly stable full-consensus ankyrin repeat proteins. J Mol Biol 2008;376:241–57.
22. Greenwald RB, Choe YH, McGuire J, Conover CD. Effective drug delivery by PEGylated drug conjugates. Adv Drug Deliv Rev 2003;55:217–50.
23. Zahnd C, Pécorari F, Straumann N, Wyler E, Plückthun A. Selection and characterization of Her2 binding-designed ankyrin repeat proteins. J Biol Chem 2006;281:35167–75.
24. Zahnd C, Wyler E, Schwenk JM, et al. A designed ankyrin repeat protein evolved to picomolar affinity to Her2. J Mol Biol 2007;369:1015–28.
25. Steiner D, Forrer P, Plückthun A. Efficient selection of DARPins with sub-nanomolar affinities using SRP phage display. J Mol Biol 2008;382:1211–27.
26. Kubetzko S, Balic E, Waibel R, Zangemeister-Wittke U, Plückthun A. PEGylation and multimerization of the anti-p185HER-2 single chain Fv fragment 4D5: effects on tumor targeting. J Biol Chem 2006;281:35186–201.
27. Waibel R, Alberto R, Willuda J, et al. Stable one-step technetium-99m labeling of His-tagged recombinant proteins with a novel Tc(I)-carbonyl complex. Nat Biotechnol 1999;17:897–901.

28. Kubetzko S, Sarkar CA, Plückthun A. Protein PEGylation decreases observed target association rates via a dual blocking mechanism. Mol Pharmacol 2005;68:1439–54.
29. Tang Y, Wang J, Scollard DA, et al. Imaging of HER2/neu-positive BT-474 human breast cancer xenografts in athymic mice using ^{111}In-trastuzumab (Herceptin) Fab fragments. Nucl Med Biol 2005; 32:51–8.
30. Gerstner RB, Carter P, Lowman HB. Sequence plasticity in the antigen-binding site of a therapeutic anti-HER2 antibody. J Mol Biol 2002;321:851–62.
31. Schott ME, Milenic DE, Yokota T, et al. Differential metabolic patterns of iodinated versus radiometal chelated anticarcinoma single-chain Fv molecules. Cancer Res 1992;52:6413–7.
32. Berndorff D, Borkowski S, Sieger S, et al. Radioimmunotherapy of solid tumors by targeting extra domain B fibronectin: identification of the best-suited radioimmunoconjugate. Clin Cancer Res 2005; 11:7053–63s.
33. Gainkam LO, Huang L, Caveliers V, et al. Comparison of the biodistribution and tumor targeting of two ^{99m}Tc-labeled anti-EGFR nanobodies in mice, using pinhole SPECT/micro-CT. J Nucl Med 2008;49: 788–95.
34. Kohl A, Binz HK, Forrer P, Stumpp MT, Plückthun A, Grütter MG. Designed to be stable: crystal structure of a consensus ankyrin repeat protein. Proc Natl Acad Sci U S A 2003;100:1700–5.
35. Willuda J, Honegger A, Waibel R, et al. High thermal stability is essential for tumor targeting of antibody fragments: engineering of a humanized anti-epithelial glycoprotein-2 (epithelial cell adhesion molecule) single-chain Fv fragment. Cancer Res 1999;59:5758–67.
36. Schmidt MM, Wittrup KD. A modeling analysis of the effects of molecular size and binding affinity on tumor targeting. Mol Cancer Ther 2009;8:2861–71.
37. Adams GP, Tai M-S, McCartney JE, et al. Avidity-mediated enhancement of *in vivo* tumor targeting by single-chain Fv dimers. Clin Cancer Res 2006;12:1599–605.
38. Adams GP, Schier R, McCall AM, et al. Prolonged *in vivo* tumour retention of a human diabody targeting the extracellular domain of human HER2/neu. Br J Cancer 1998;77:1405–12.
39. Matsumura Y, Maeda H. A new concept for macromolecular therapeutics in cancer chemotherapy: mechanism of tumoritropic accumulation of proteins and the antitumor agent smancs. Cancer Res 1986;46:6387–92.
40. Greish K, Fang J, Inutsuka T, Nagamitsu A, Maeda H. Macromolecular therapeutics: advantages and prospects with special emphasis on solid tumour targeting. Clin Pharmacokinet 2003;42:1089–105.
41. Nielsen UB, Adams GP, Weiner LM, Marks JD. Targeting of bivalent anti-ErbB2 diabody antibody fragments to tumor cells is independent of the intrinsic antibody affinity. Cancer Res 2000;60:6434–40.
42. Deyev SM, Waibel R, Lebedenko EN, Schubiger AP, Plückthun A. Design of multivalent complexes using the barnase*barstar module. Nat Biotechnol 2003;21:1486–92.
43. Graff CP, Wittrup KD. Theoretical analysis of antibody targeting of tumor spheroids: importance of dosage for penetration, and affinity for retention. Cancer Res 2003;63:1288–96.
44. Wikman M, Steffen AC, Gunneriusson E, et al. Selection and characterization of HER2/neu-binding affibody ligands. Protein Eng Des Sel 2004;17:455–62.
45. Tolmachev V, Nilsson FY, Widström C, et al. ^{111}In-benzyl-DTPA-ZHER2:342, an affibody-based conjugate for *in vivo* imaging of HER2 expression in malignant tumors. J Nucl Med 2006;47: 846–53.
46. Orlova A, Nilsson FY, Wikman M, et al. Comparative *in vivo* evaluation of technetium and iodine labels on an anti-HER2 affibody for single-photon imaging of HER2 expression in tumors. J Nucl Med 2006; 47:512–9.
47. Dreher MR, Liu W, Michelich CR, Dewhirst MW, Yuan F, Chilkoti A. Tumor vascular permeability, accumulation, and penetration of macromolecular drug carriers. J Natl Cancer Inst 2006;98:335–44.
48. Taylor AE, Granger DN. Exchange of macromolecules across the microcirculation. In: Renkin E, Michel CC, editors. Handbook of physiology microcirculation: Am Physiol Soc. Bethesda (MD): 1984, p. 467–520.
49. Phillips RJ. A hydrodynamic model for hindered diffusion of proteins and micelles in hydrogels. Biophys J 2000;79:3350–3.
50. Yuan F, Dellian M, Fukumura D, et al. Vascular permeability in a human tumor xenograft: molecular size dependence and cutoff size. Cancer Res 1995;55:3752–6.